Single crystal growth of apatite-type Al-doped neodymium silicates by the floating zone method

An, Tao; Baikie, Tom; Wei, Fengxia; Li, Henan; Brink, Frank; Wei, Jun; Ngoh, Shwu Lan; White, Timothy John; Kloc, Christian

2011

https://hdl.handle.net/10356/85586

https://doi.org/10.1016/j.jcrysgro.2011.08.010

Single crystal growth of apatite-type Al-doped neodymium silicates by the floating zone method

Tao An[a], Tom Baikie[a], Fengxia Wei[a], Henan Li[a], Frank Brink[b], Jun Wei[c], Shwu Lan Ngoh[c], Timothy J. White[b], Christian Kloc[a,*]

[a]School of Materials Science and Engineering, Nanyang Technological University, Block N4.1, Nanyang Avenue, Singapore 639798.

[b]Centre for Advanced Microscopy, The Australian National University, Canberra ACT 0200, Australia.

[c]Singapore Institute of Manufacturing Technology,71 Nanyang Drive, Singapore 638075.

[*]Corresponding author. Tel.: +65 6790 4716. E-mail address: ckloc@ntu.edu.sg (C. Kloc).

**Abstract**

Large lanthanoid silicates ($Ln_{9.33}Si_6O_{26}$) adopt the hexagonal apatite structure and show potential as solid oxide fuel cell (SODC) electrolytes due to their high oxide ion conductivity at intermediate temperatures (500 – 700°C). Ions migrate preferentially along the crystallographic c axis, and can be improved by introducing lower valent elements at the silicon sites. To better understand this phenomenon, single crystals of aluminum-doped neodymium silicate $Nd_{9.33+x/3}Al_xSi_{6-x}O_{26}$ ($0 \leq x \leq 1$) were grown using the floating-zone method in an inert environment at a growth rate of 5 mm/L. The products with $x < 1.5$ were homogeneous, transparent and crack-free crystals. For $x = 1.5$ the monophasic crystal contained minor cracks after cooling and for $x = 2$ a two phase (apatite + $NdAlO_3$) polycrystalline mass was obtained. The quality of the $0 \leq x \leq 1.5$ crystals were confirmed by neutron diffraction and synchrotron X-ray rocking curve diffraction. The incorporation of aluminum into apatite at nominal concentrations was independently confirmed by energy dispersive X-ray spectroscopy (EDX) and electron backscatter diffraction (EBSD) found the crystallographic habit showed extension along [001].

1. Introduction

The development of apatite electrolytes is driven by the need to reduce the high operating temperatures (~1000°C) of current generation solid oxide fuel cells (SOFC) and thereby extend their operating life. The benchmark material, yttria-stabilized zirconia (YSZ), only shows significant ionic conductivity (~ 0.1 Scm^{-1}) from 900 – 1000°C [1, 2], which drops quickly as temperature is lowered (~10^{-3} Scm^{-1} at 500°C) [3]. Hexagonal lanthanoid silicates of the apatite structural family with ideal formula $Ln_{9.33}Si_6O_{26}$ offer better performance at intermediate temperatures (500 – 700°C) [4]. For example, sintered polycrystalline $La_{9.33}Si_6O_{26}$ displays ionic conductivity as high as 4.3×10^{-3} Scm^{-1} at 500°C [5]. Transport is anisotropically enhanced along the hexagonal c axis, with the flux further improved by introducing lower valent ions at the tetrahedral SiO_4 (ionic radius of Si^{4+} = 0.26Å), such as Mg^{2+} (0.57Å) and Al^{3+} (0.39Å) [6, 7]. Mg expands the lattice which facilitates oxide ion transport [8], while Al doping increases the La occupancy to an optimum level for conduction [9].

The chemical formula of $Ln_{9.33}Si_6O_{26}$ can be recast as $(La_{9.33}\square_{0.67})Si_6O_{26}$, where "$\square$" represents vacancies at the Ln sites. If Al^{3+} is introduced in place of Si^{4+}, charge neutrality is maintained by decreasing Ln vacancies (assuming a fixed oxygen content):

$$(Ln_{9.33}\square_{0.67})Si_6O_{26} + xAl^{3+} \longrightarrow (Ln_{9.33+x/3}\square_{0.67-x/3})Al_xSi_{6-x}O_{26} \qquad (1)$$
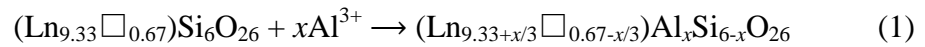
with integral stoichiometry achieved for x = 2 and $Nd_{10}Al_2Si_4O_{26}$. However, it is also possible that substitution of Si^{4+} by Al^{3+} leads to a decrease of oxide ion concentration:

$$O^{2-} + 2Si^{4+} \longrightarrow \square_{O^{2-}} + 2Al^{3+} \qquad (2)$$
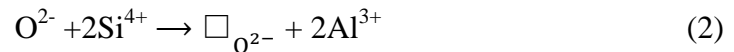
In contrast to the oxygen vacancy mechanism found for YSZ ($2Zr^{4+} + O^{2-} \longrightarrow 2Y^{3+} + \square_{O^{2-}}$) [10], the oxide ions in apatites migrate via an interstitial pathway [11]. However, most studies on the conductive properties of apatite electrolytes have been performed with pelletised and sintered polycrystalline powders, where pores and grain boundaries strongly attenuate O^{2-} transport [12]. In addition, sintered pellets inevitably display isotropic properties, although the apatite structure is intrinsically predisposed to anisotropic transport. Therefore, fundamental measurements of the magnitude of oxide

ion conductivity as a function of temperature, and the investigation of migration mechanisms require large single crystals. The floating-zone method can grow appreciable single crystals of pure and alkaline earth doped lanthanoid silicates [13 – 15], but compositions containing lower valent elements at Si sites have not been demonstrated.

Here we describe the preparation of large crystals of Al-doped neodymium silicate, $Nd_{9.33+x/3}Al_xSi_{6-x}O_{26}$, x = 0, 0.5, 1, 1.5, using the optical floating zone method, and find a solid solution limit for Al at $1.5 \leq x \leq 2$. Neodymium was chosen over more common lanthanum, as the blue colour of the former better absorbed infrared radiation that improved heat transfer and single crystal growth. The crystals were homogeneous and acicular, with extension along the c axis and the narrow full-width at half-maximum (FWHM) peaks observed rocking curve diffraction indicate a coherent domain mosaic. These crystals were therefore of sufficient quality for the assessment of ionic conductivity and structural analysis as described elsewhere [16].

2. Experimental procedures

2.1. Synthesis of polycrystalline $Nd_{9.33+x/3}Al_xSi_{6-x}O_{26}$ feed rods

Nd_2O_3 (Alfa Aesar, 99.9%), SiO_2 (Alfa Aesar, 99.9%) and Al_2O_3 (Fluka, 99.7%) were homogenised in stoichiometric ratios by hand grinding in an agate mortar and pestle. These mixtures were calcined (1200°C/10h/air), cooled to room temperature and re-ground manually for 1 hour. The product was loaded in a latex balloon and isostatically pressed into a rod (10 mm diameter and 30-40 mm in length) with a hydraulic press (200 MPa), before reactive sintering (1650°C/20h/air) to obtain feed rods (7-8 mm diameter and 30-40 mm in length).

2.2. Synthesis of seed crystal

In reconnaissance studies, polycrystalline rods were deployed as seeds for the growth of pure neodymium silicate. The tabular, as-grown crystals were facetted and inspection by synchrotron X-ray diffraction found the parallel surfaces contained (0 0 l), l = 2n, peaks only. When thin sections were viewed in [001] under crossed polarisers, complete

extinction confirmed the material was a single crystal. These $Nd_{9.33}Si_6O_{26}$ apatite crystals were used to seed the growth of undoped and Al-doped neodymium silicate apatites, and orientated such that preferred growth was parallel to the *c* axis.

2.3. Crystal growth

An FZ-T-4000-H-VPO-VII-PC optical floating zone furnace (Crystal Systems Corporation, Japan) was used, with four 1.5 kW halogen lamps and corresponding ellipsoidal mirrors that focus the infrared irradiation to a small region. A constant flow of argon (2 L/min) was passed through the chamber during growth. As the feed and seed rod tips start to melt, they are brought into contact to form the floating-zone; after the molten zone stabilises, the entire mirror stage translates upwards (5 mm/h) during crystal growth. The rods are counter-rotated at constant speed (40 rpm) to maintain a stable and well mixed molten zone.

2.4. Methods of crystal characterisation

A disc (5mm × 2mm) was cut from each crystal perpendicular to the hexagonal basal plane, embedded in epoxy resin and manually polished to a mirror finish using 0.06 μm colloidal silica polishing suspension (Buehler). A Zeiss UltraPlus field emission scanning electron microscope (FESEM) equipped with an HKL electron backscatter diffraction (EBSD) system further confirmed the growth direction. Given the possibility of compositional change during crystal growth, analytical scanning electron microscopy was used to validate the incorporation of aluminium. The energy-dispersive X-ray analysis (EDX) was carried out at 15kV using a JEOL JSM-7600F FESEM equipped with an Oxford Instrument XMax Silicon Drift Detector and INCA Software.

The central portions of the single crystals (~5mm long) were cut and manually ground for analysis by powder X-ray diffraction (PXRD) to confirm apatite was synthesised and identify secondary phases. Patterns were collected on a Bruker D8 Advance diffractometer using Cu *Kα* X-rays generated at 40 kV and 40 mA. The crushed powders were filled in a top-loaded trough and pressed with a glass slide to have a flat surface. The data were accumulated from 10 – 130° 2θ using a step size of 0.02° with a dwell

time of 1.2s per step. Under these conditions the intensity of the strongest reflection was approximately 9000 – 12500 counts.

Neutron diffraction patterns were collected at 100K on the Koala Laue diffractometer beam line at the OPAL reactor operated by the Australian Nuclear Science and Technology Organisation (ANSTO) to establish crystal quality. Laue diffraction employed polychromated thermal-neutron beam coupled with a large solid-angle (8 steradians) cylindrical image-plate detector. The apatite crystals were broken into approximate $1.5 \times 1.5 \times 1.5$ mm dimensions and mounted on an aluminium pin with silicon grease.

The rocking curves of the crystals were measured with a Bruker Smart Apex II three-circle diffractometer using graphite monochromated Mo $K\alpha$ radiation over the angular range 5 - 55° 2θ to find the mosaic spread of the crystals.

3. Results and Discussion

All crystals were homogeneous, transparent and violet, and approximately 5 mm in diameter and 20-25 mm in length (Fig. 1). The $Nd_{9.33}Si_6O_{26}$, $Nd_{9.50}Al_{0.5}Si_{5.5}O_{26}$ and $Nd_{9.67}AlSi_5O_{26}$ crystals were free of fractures, but the $Nd_{9.83}Al_{1.5}Si_{4.5}O_{26}$ crystal contained some cracks that formed during cooling from the crystallographic stresses induced by the greater amount of Al. The crystal cross-sections display clear hexagonal faceting, which is uncommon for crystals grown by this optical floating zone method due to the high thermal gradients. For "$Nd_{10}Al_2Si_4O_{26}$", the melt solidified as a polycrystalline rod.

Neutron diffraction of the bulk crystals yielded reflections without splitting, that could be indexed as hexagonal $P6_3/m$ apatite, thus excluding lower symmetries that are sometimes reported for rare earth silicate apatites [6]. This also confirmed the entire volume of each inspected crystal consisted of a single grain.

Rietveld analysis of powdered single crystals using $P6_3/m$ yielded good fits with no evidence of secondary phases, while a small amount (6.44 wt%) of neodymium aluminate ($NdAlO_3$) was identified from the as-grown polycrystalline "$Nd_{10}Al_2Si_4O_{26}$" (Fig. 2). The

refined data are summarised in Table 1. The unit cells dilated as the composition became increasingly aluminous. Vegard's Law was not obeyed (Fig. 3) suggesting the simple altervalent substitution of equation (1) is augmented by the creation of oxygen vacancies (equation (2)) at high aluminium content. This successful displacement of Si^{4+} by Al^{3+} was independently confirmed by analytical SEM of these crystals (Fig. 4), with the intensity of the Al X-rays increasing as Si decreased. In addition, for each sample, $6 - 8$ areas were inspected by EDX and quantitation gave values conforming to the nominal compositions within error, also confirming homogeneity. The crystallographic orientation of the crystal cross-sections was shown by EBSD to be within a few degrees of [001] (Fig. 5).

Rocking curves measurements were carried out on the (4 4 2) reflection to further study crystal quality. The $Nd_{9.33}Si_6O_{26}$ yielded a FWHM of $0.22°$, $Nd_{9.50}Al_{0.5}Si_{5.5}O_{26}$ and $Nd_{9.83}Al_{1.5}Si_{4.5}O_{26}$ gave $0.20°$, and $Nd_{9.67}AlSi_5O_{26}$ showed the narrowest FWHM of $0.18°$. These values are comparable to those previously reported for Nd oxide single crystals grown [17].

4. Conclusion

The floating zone method was used to prepare large ($5 \times 20 - 25$ mm) crystals of neodymium silicate apatite and its aluminum doped analogues $Nd_{9.33+x/3}Al_xSi_{6-x}O_{26}$, $x = 0$, 0.5, 1.0, 1.5, that were homogeneous, transparent, and free of macroscopic cracks except at the highest aluminium content (nominally $Nd_{10}Al_{1.5}Si_{4.5}O_{26.25}$). The solid solution limit may be somewhat less than the theoretical composition of $x = 2$. Subsequent inspection with neutron diffraction and EBSD confirmed their single crystal nature and established preferred growth along the c axis. Powder XRD showed that up to $x \sim 1.5$ the products were monophasic with unit cell parameters increasing with x, however it is noted that Vegard's Law is not obeyed, suggesting that Al^{3+} displacement of Si^{4+} is accompanied by both the infilling of Nd vacancies and the creation of oxygen vacancies. The incorporation of aluminium was validated by analytical scanning electron microscopy, and rocking curve measurements provided further evidence of high crystal quality. The

crystals of $Nd_{10}Si_6O_{27}$, $Nd_{10}Al_{0.5}Si_{5.5}O_{26.75}$, $Nd_{10}AlSi_5O_{26.5}$, and $Nd_{10}Al_{1.5}Si_{4.5}O_{26.25}$ (the region without cracks) are suitable for the measurement of ionic conductivity, specifically as a function of crystallographic orientation, and are presently the subject of further investigation.

References

[1] L. Carrette, K.A. Friedrich, U. Stimming, Fuel Cells - Fundamentals and Applications, Fuel Cells, 1 (2001) 5-39.

[2] T. Ishihara, N.M. Sammes, O. Yamamoto, Electrolytes, in: S. Singhal, K. Kendall (Eds.) High Temperature Solid Oxide Fuel Cells: Fundamentals, Design and Applications, Elsevier, Oxford, 2003, pp. 83-117.

[3] V.V. Kharton, F.M.B. Marques, A. Atkinson, Transport properties of solid oxide electrolyte ceramics: a brief review, Solid State Ionics, 174 (2004) 135-149.

[4] S. Nakayama, T. Kagayama, H. Aono, Y. Sadoaka, Ionic conductivity of lanthanoid silicates, $Ln_{10}(SiO_4)_6O_3$ (Ln = La, Nd, Sm, Gd, Dy, Y, Ho, Er and Yb), J. Mater. Chem., 11 (1995) 1801-1806.

[5] S. Nakayama, M. Sakamoto, Electrical properties of new type high oxide ionic conductor $RE_{10}Si_6O_{27}$ (RE = La, Pr, Nd, Sm, Gd, Dy), Journal of the European Ceramic Society, 18 (1998) 1413-1418.

[6] P.R. Slater, J.E.H. Sansom, J.R. Tolchard, Development of apatite-type oxide ion conductors, Chem. Rec., 4 (2004) 373-384.

[7] R.D. Shannon, Revised effective ionic radii and systematic studies of interatomic distances in halides and chalcogenides, Acta Crystallographica Section A, 32 (1976) 751-767.

[8] H. Yoshioka, Y. Nojiri, S. Tanase, Ionic conductivity and fuel cell properties of apatite-type lanthanum silicates doped with Mg and containing excess oxide ions, Solid State Ionics, 179 (2008) 2165-2169.

[9] E.J. Abram, D.C. Sinclair, A.R. West, A novel enhancement of ionic conductivity in the cation-deficient apatite $La_{9.33}(SiO_4)_6O_2$, Journal of Materials Chemistry, 11 (2001) 1978-1979.

[10] N.Q. Minh, Ceramic Fuel Cells, Journal of the American Ceramic Society, 76 (1993) 563-588.

[11] E. Kendrick, M.S. Islam, P.R. Slater, Developing apatites for solid oxide fuel cells: insight into structural transport and doping properties, J. Mater. Chem., 17 (2007) 3104-3111.

[12] M. Higuchi, Y. Masubuchi, S. Nakayama, S. Kikkawa, K. Kodaira, Single crystal growth and oxide ion conductivity of apatite-type rare-earth silicates, Solid State Ionics, 174 (2004) 73-80.

[13] M. Higuchi, K. Kodaira, S. Nakayama, Growth of apatite-type neodymium silicate single crystals by the floating-zone method, Journal of Crystal Growth, 207 (1999) 298-302.

[14] M. Higuchi, H. Katase, K. Kodaira, S. Nakayama, Float zone growth and characterization of $Pr_{9.33}(SiO_4)_6O_2$ and $Sm_{9.33}(SiO_4)_6O_2$ single crystals with an apatite structure, Journal of Crystal Growth, 218 (2000) 282-286.

[15] Y. Masubuchi, M. Higuchi, H. Katase, T. Takeda, S. Kikkawa, K. Kodaira, S. Nakayama, Oxide ion conduction in $Nd_{9.33}(SiO_4)_6O_2$ and $Sr_2Nd_8(SiO_4)_6O_2$ single crystals grown by floating zone method, Solid State Ionics, 166 (2004) 213-217.

[16] T. Baikie, T. An, F. Wei, S.S. Pramana, M.K. Schreyer, R.O. Piltz, C. Kloc, P.R. Slater, T.J. White, A single crystal study of oxide ion conducting apatite electrolytes, in preparation, (2011).

[17] Y. Wang, S. Cao, M. Shao, S. Yuan, B. Kang, J. Zhang, A. Wu, J. Xu, Growth rate dependence of the $NdFeO_3$ single crystal grown by float-zone technique, Journal of Crystal Growth, 318 (2011) 927-931.

Table Caption(s)

Table 1   Refined unit cell parameters and reliability indices for the pulverised single crystals obtained by Rietveld analysis.
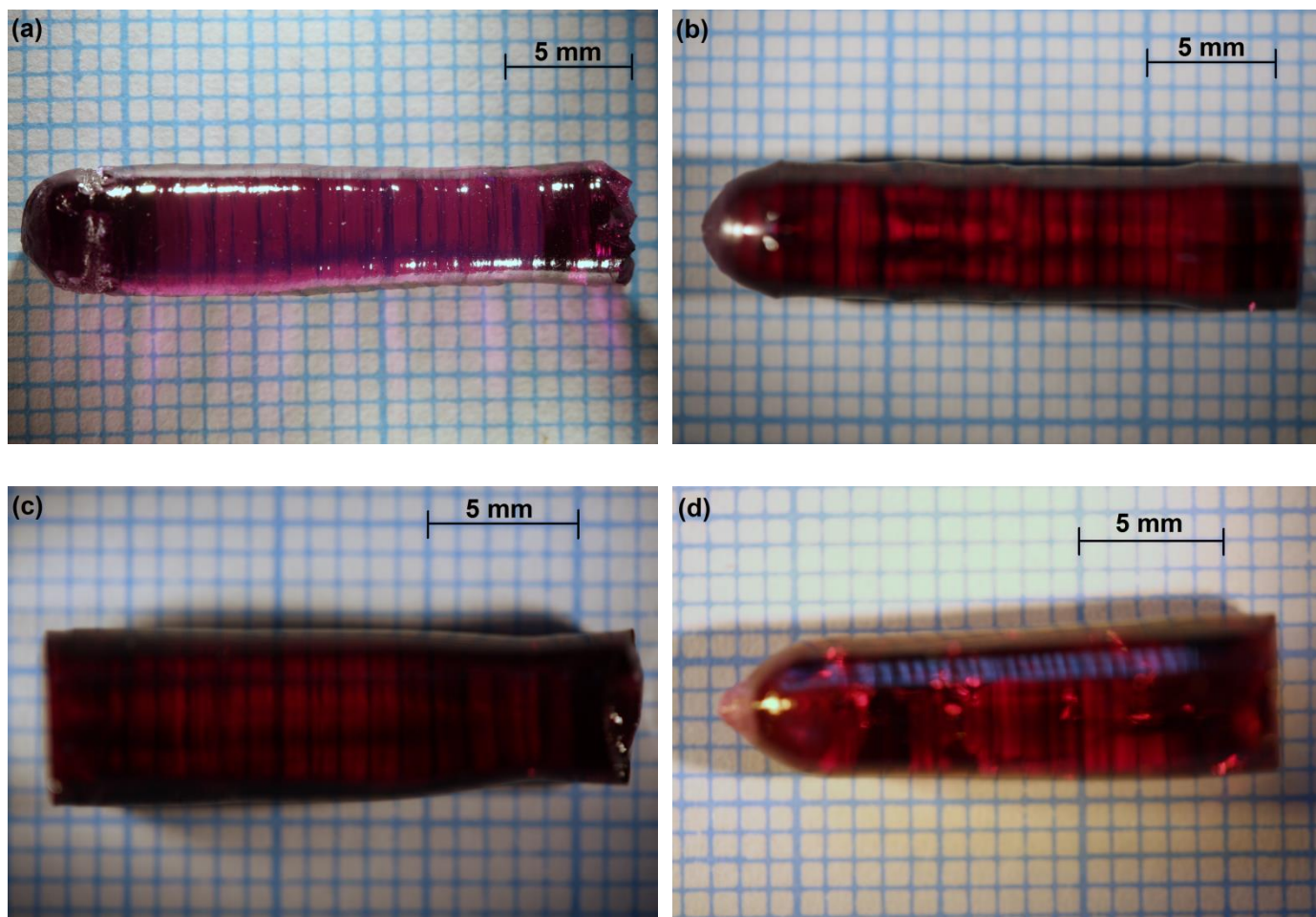
Figure Caption(s)

Figure 1   Crystals of (a) $Nd_{9.33}Si_6O_{26}$, (b) $Nd_{9.50}Al_{0.5}Si_{5.5}O_{26}$, (c) $Nd_{9.67}AlSi_5O_{26}$ and (d) $Nd_{9.83}Al_{1.5}Si_{4.5}O_{26}$ with extension along the crystallographic c axis.

Figure 2   Rietveld plots of powder X-ray diffraction patterns of (a) $Nd_{9.83}Al_{1.5}Si_{4.5}O_{26}$ and (b) "$Nd_{10}Al_2Si_4O_{26}$" in the $20 - 40°$ range. While the pattern of $Nd_{9.83}Al_{1.5}Si_{4.5}O_{26}$ contains peaks from the $P6_3/m$ apatite only, major $NdAlO_3$ reflections, (0 1 2) at 23.70°, ($\bar{1}$ 2 0) at 33.65° and ($\bar{1}$ 1 4) at 33.87°, were identified in "$Nd_{10}Al_2Si_4O_{26}$".

Figure 3   Unit cell parameters **a** and **c** as a function of Al content. To $x = 1.5$, the crystals are single-phase apatite, beyond which $NdAlO_3$ appears as a secondary phase.

Figure 4   The EDX spectra of $Nd_{28+x/3}Al_xSi_{6-x}O_{26}$ crystals with $x = 0$, 0.5, 1.0 and 1.5 showing the $K\alpha$ peaks of Al (1.487 keV) and Si (1.740 keV). Six to eight separate regions of each crystal were inspected in [001] cross-section to obtain the averaged plots shown.

Figure 5   A representative EBSD pattern of $Nd_{9.67}AlSi_5O_{26}$. Other compositions gave similar patterns of identical crystallographic orientation.

Table 1

Refined unit cell parameters and reliability indices for the pulverised single crystals obtained by Rietveld analysis.

	$Nd_{9.33}Si_6O_{26}$	$Nd_{9.50}Al_{0.5}Si_{5.5}O_{26}$	$Nd_{9.67}AlSi_5O_{26}$	$Nd_{9.83}Al_{1.5}Si_{4.5}O_{26}$	$Nd_{10}Al_2Si_4O_{26}$
Unit cell parameters					
a (Å)	9.5727(3)	9.5738(1)	9.57724(7)	9.58457(7)	9.59159(7)
c (Å)	7.0250(2)	7.05125(8)	7.06499(6)	7.07102(6)	7.06824(6)
Volume (Å³)	557.51(4)	559.71(1)	561.21(1)	562.55(1)	563.148(9)
Reliability Indices					
R_{wp}	4.66%	4.79%	4.41%	4.41%	3.69%
R_p	3.54%	3.63%	3.39%	3.40%	2.89%
χ^2	1.48	1.43	1.46	1.49	1.28
R_B	1.91%	2.57%	2.10%	1.46%	1.25%
R_{exp}	3.15%	3.34%	3.01%	2.96%	2.89%

Fig. 1. Crystals of (a) $Nd_{9.33}Si_6O_{26}$, (b) $Nd_{9.50}Al_{0.5}Si_{5.5}O_{26}$, (c) $Nd_{9.67}AlSi_5O_{26}$ and (d) $Nd_{9.83}Al_{1.5}Si_{4.5}O_{26}$ with extension along the crystallographic c axis.
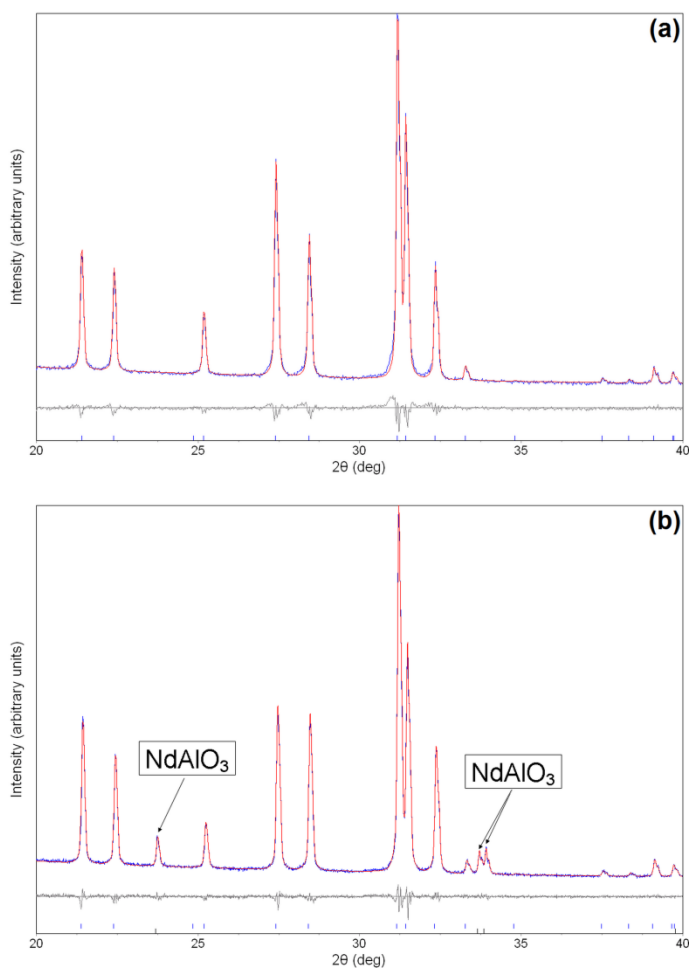
Fig. 2. Rietveld plots of powder X-ray diffraction patterns of (a) $Nd_{9.83}Al_{1.5}Si_{4.5}O_{26}$ and (b) "$Nd_{10}Al_2Si_4O_{26}$" in the 20 – 40° range. While the pattern of $Nd_{9.83}Al_{1.5}Si_{4.5}O_{26}$ contains peaks from the $P6_3/m$ apatite only, major $NdAlO_3$ reflections, (0 1 2) at 23.70°, ($\bar{1}$ 2 0) at 33.65° and ($\bar{1}$ 1 4) at 33.87°, were identified in "$Nd_{10}Al_2Si_4O_{26}$".
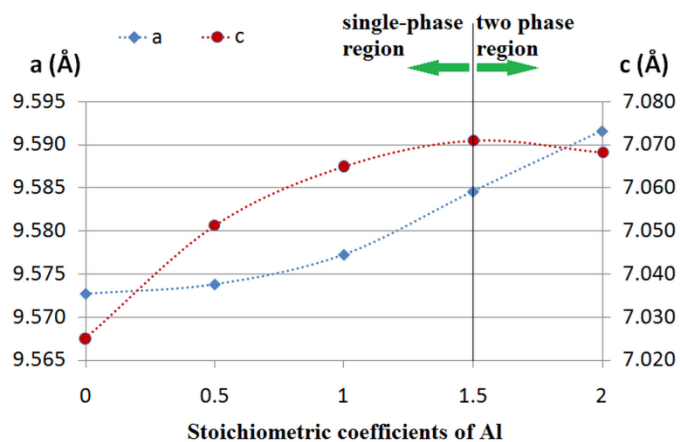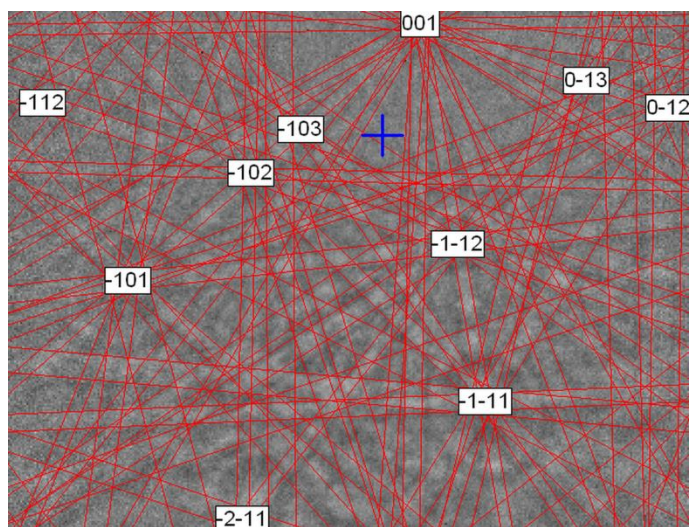
Fig. 3. Unit cell parameters **a** and **c** as a function of Al content. To $x = 1.5$, the crystals are single-phase apatite, beyond which $NdAlO_3$ appears as a secondary phase.
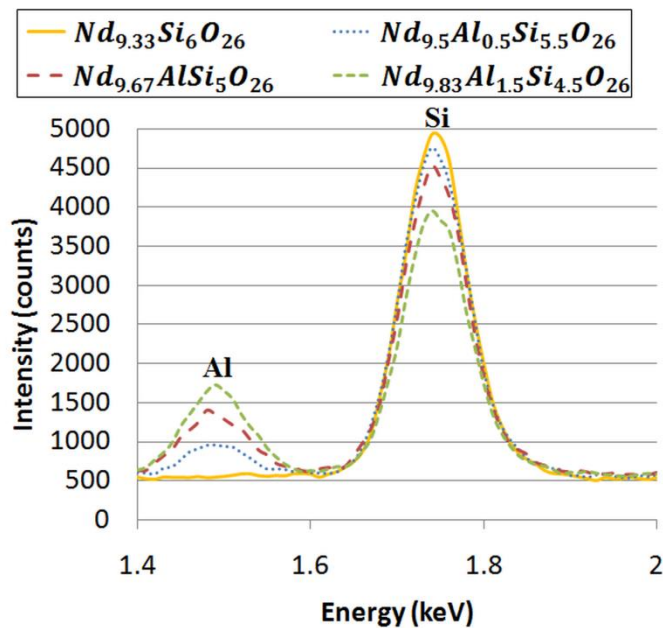
Fig. 4. The EDX spectra of $Nd_{28+x/3}Al_xSi_{6-x}O_{26}$ crystals with $x = 0, 0.5, 1.0$ and 1.5 showing the $K\alpha$ peaks of Al (1.487 keV) and Si (1.740 keV). Six to eight separate regions of each crystal were inspected in [001] cross-section to obtain the averaged plots shown.

Fig. 5. A representative EBSD pattern of $Nd_{9.67}AlSi_5O_{26}$. Other compositions gave similar patterns of identical crystallographic orientation.